Identifiability of parameters of three-phase oil relative permeability models under simultaneous water and gas (SWAG) injection

Ehsan Ranaee[1*], Leili Moghadasi[1], Fabio Inzoli[1], Monica Riva[2,3], Alberto Guadagnini[2,3]

[1]Dipartimento di Energia, Politecnico di Milano, Via Lambruschini 4, 20156 Milano, Italy

[2]Dipartimento di Ingegneria Civile e Ambientale, Politecnico di Milano, Piazza L. Da Vinci 32, 20133 Milano, Italy

[3]Department of Hydrology and Atmospheric Sciences, University of Arizona, Tucson, Arizona 85721, USA

* Corresponding author: Tel. +39 02 2399 3826. Fax. +39 02 2399 3913

E–mail address: ehsan.ranaee@polimi.it

Complete reference: Ranaee, E., L. Moghadasi, F. Inzoli, M. Riva, and A. Guadagnini (2017), Identifiability of parameters of three-phase oil relative permeability models under simultaneous water and gas (SWAG) injection, *J. Petrol. Sci. Eng.*, 159, 1-10, doi:10.1016/j.petrol.2017.09.062

Abstract

We assess the relative performance of a suite of selected models to interpret three-phase oil relative permeability data and provide a quantification of the identifiability of the model parameters. We ground our analysis on observations of Steady-State two- and three-phase relative permeabilities we collect on a water-wet Sand-Pack sample through series of core-flooding experiments. Three-phase experiments are characterized by simultaneous injection of water and gas (SWAG) phases into the core sample initiated at irreducible water saturation, a scenario which is relevant for modern enhanced oil recovery techniques. The selected oil relative permeability models include classical and recent formulations and we consider their performance when (*i*) solely two-phase data are employed to render predictions of three-phase oil relative permeability (k_{ro}), and/or (*ii*) two- and three-phase data are jointly used for model calibration. A maximum likelihood (ML) approach is employed to estimate model parameters in the latter case. We assess identifiability of model parameters through the Profile Likelihood (PL) technique. We rely on formal model discrimination criteria for a quantitative evaluation of the interpretive skill of each of the candidate models tested. We also evaluate the relative degree of likelihood associated with the competing models through a posterior probability weight and use ML Bayesian model averaging (BMA) to provide model-averaged estimate of k_{ro} and the associated uncertainty bounds.

Results show evaluating identifiability of uncertain parameters to the available dataset can provide us valuable information about the quality of the parameters estimations, thus inferring which model predictions are feasible. Such analysis can reduces computational costs by selecting solely identifiable models among available candidates on the basis of an available dataset. In some cases, PL technique yields more feasible predictions of the estimating parameters confidence intervals compared to the ones resulting from the analysis of covariance matrix of ML estimation errors.

Keywords: relative permeability, parameter estimations, maximum likelihood, model discrimination criteria, model averaging, profile likelihood, identifiability analysis.

1 Introduction

Proper characterization of flow under three-phase conditions is critical for a variety of field oriented industrial and environmental applications, including oil production projects and their impacts on groundwater resources. Multiphase flow in porous media may potentially occur in hydrocarbon production scenarios and modern enhanced oil recovery (EOR) techniques based on simultaneous (or cyclic) injection of water and gas phases into an oil reservoir causes three-phase flow to take place through some regions of the system. In this context, adequate characterization of fluid phases relative permeabilities is of critical importance, since formulations based on analogies to Darcy's Law are routinely employed for the continuum-scale simulation of multiphase flow dynamics in porous/fractured media (e.g., Silpngarmlers et al. 2002 and references therein). A reliable characterization (either experimental or theoretical) of relative permeabilities, including a quantification of estimation uncertainty, enables us to assess the performance and efficiency of the reservoir production under the application of EOR techniques and the repercussions that these might have on the general subsurface flow circulation pattern, which is a key environmental concern in modern applications.

All these elements should be contrasted with the observation that experimental set-ups of three-phase flow systems are remarkably complex, costly, and time-consuming to design and operate. Due to a combination of these reasons, documentation and availability of three-phase relative permeability experiments is scarce (see, e.g., Oak 1990; Blunt 2000; Alizadeh and Piri 2014a). A variety of empirical/semi-empirical models have been proposed for the characterization of three-phase relative permeabilities (Spiteri and Juanes 2004; Ranaee et al. 2016 and references therein). Ranaee et al (2016) jointly employ Maximum Likelihood (ML) parameter estimation and model identification criteria to study the performance of a set of three-phase relative permeability models to interpret laboratory core-flooding datasets presented by Alizadeh and Piri (2014b). The datasets analyzed include the dependence on phase saturation of two- and three-phase relative permeabilities collected under cyclic water alternating gas (WAG) injection scenarios. A key conclusion of the analysis of Ranaee et al. (2016) is that the recent three-phase oil relative permeability model (termed Sigmoid model) proposed by Ranaee et al. (2015) has a clear potential to outperform the other models analyzed. The need for additional testing against data-set acquired under different conditions is highlighted by the authors to support the robustness of such a model. This is precisely one of the objectives of the current work. As such, we ground our analysis on the recent core-flooding data-sets presented by Moghadasi et al. (2016) and collected under simultaneous injection of water and gas (SWAG) phases. The data we analyze involve Steady-State two- and three-phase laboratory experiments performed on a quartz Sand-Pack sample.

Another objective of our study is related to the assessment of the degree of reliability and/or ambiguity of the results of optimization/calibration of the relative permeability models considered in the presence of given experimental information content. In this sense, it is important to infer the reliability associated with the estimated model parameters on the basis of the amount and quality of available data (e.g., Flassig et al. 2015) and to quantify the sensitivity of available data and/or model responses to the variation of uncertain model parameters (e.g., Tiedeman et al. 2003, 2004; Ting et al. 2015 and references therein). One then needs to assess the way parameter estimation uncertainty propagates onto bounds of uncertainty for model predictions (Kreutz et al. 2012 and references therein). We tackle these issues, including identifiability of model parameters, in the framework of a local sensitivity analysis (SA) on a selected suite of models. The challenges associated with the analysis are amplified by the type of flow process we consider and by the way the multi-phase flow physics are embedded (to various degrees) into each of the interpretive models we consider.

On these bases, here we consider a collection of empirical models (i.e., the models proposed by Stone 1970; Baker 1988; Du et al. 2004; and Ranaee et al. 2015) of three-phase oil relative permeability, k_{ro}, and: (*i*) rely on a Maximum Likelihood (ML) approach to compare the individual skill of each of these models to interpret the k_{ro} data of Moghadasi et al. (2016); (*ii*) quantify the uncertainties associated with ML parameter estimates for each model; (*iii*) perform a comprehensive local sensitivity analysis for all model parameters; (*iv*) study the manifestation of possible structural and/or practical non-identifiability of model parameters through the use of the Profile Likelihood (PL) technique (Raue et al. 2009); and (*v*) illustrate the ability of ML Bayesian model averaging (BMA) approaches to interpret available dataset. We treat the models considered as a set of competing alternatives, rank them through model selection (or model discrimination) criteria and evaluate the posterior probability (or weight) associated with each of them. We assess the way the uncertainty associated with identifiable models parameters propagates to model outputs, i.e., values of k_{ro}, within the framework of a multimodel analysis approach.

The work is organized as follows. Section 2.1 illustrates the experimental core-flooding setup and the collected Steady-State two- and three-phase data. The ML calibration procedure is briefly described in Section 2.2. Section 2.3 presents the Profile Likelihood (PL) technique for assessment of identifiable parameter(s) of each considered model. Section 2.4 illustrates the main features of the three-phase oil relative permeability models analyzed. Key results are presented in Section 3.

2 Material and methods

2.1 Available dataset

The test bed we select comprises a three-phase core-flooding dataset collected on a water-wet Sand-Pack (Moghadasi et al. 2016). Fig. 1 depicts a sketch of the setup employed in the experiments.

Two- and three-phase Steady-State (SS) laboratory experiments are performed by simultaneous injection of fluids into the core sample, according to the steps depicted in Fig. 2. The system state resulting from each of the steps described in the following and depicted in Fig. 2 is maintained for 24 hours to ensure attainment of equilibrium conditions. Before initiating the (two- or three-phase) experiments, the core sample is fully saturated with water. Absolute permeability of the sample to the water phase is characterized by applying a sequence of diverse flow rates and employing Darcy's law (Step A in Figs. 2a, b). Oil is then injected to displace water. This drainage process takes place until no more water is eluted from the system. The (highest) value of oil relative permeability, $\overline{k}_{row}^{M}$, is then determined at such irreducible (connate) water saturation, $\overline{S}_{wc}$, conditions (Step B in Figs. 2a, b).

Joint injection of the oil and water phases is performed for the two-phase setting by applying a total constant flow rate of 480 ml/h. The collection of experimental data is performed by increasing the water fractional flow rate while decreasing the oil fractional flow rate (Steps C-E in Fig. 2a). For a given fractional flow rate, measurements of fluid saturations and pressure drop (across the core sample) are taken at Steady-State (SS) conditions. Note that, as mentioned above, each step takes almost 24 hours to attain equilibrium. Residual oil saturation, $\overline{S}_{orw}$, is established at the end of the oil-water imbibition process, when no more oil is eluted from the core (Step F in Fig. 2a). A series of SS drainage experiments are then performed on the core sample, starting at $\overline{S}_{orw}$ and increasing oil and decreasing water fractional flow rates. The Steady-State oil-gas drainage process is also assessed through a similar experimental procedure by simultaneous injection of oil and gas (increasing gas and decreasing oil flow rates) into the core sample initiated at $\overline{S}_{wc}$.

The three-phase SS experiment is started at $\overline{S}_{wc}$ and is performed by simultaneous injections of water, oil and gas. The three-phase dataset includes oil relative permeabilities collected under an Increasing-Decreasing-Increasing saturation path (termed IDI, referring here to increasing water, decreasing oil and increasing gas fractional flow rates) and is representative reservoir behavior during a primary oil production (see Fig. 2b).

Saturation values are recorded during both two- and three-phase experiments by means of an in-situ X-Ray saturation monitoring technique. X-Ray scans of the rock sample are performed after each step for the assessment of saturation profiles. Relative permeabilities are finally calculated upon applying Darcy's law and are represented as a

function of the corresponding average core saturation determined from the X-Ray in-situ measurements (see Moghadasi et al. 2015, 2016 for additional details).

Data of oil relative permeabilities observed from (*a*) two-phase oil-water, $\overline{k}_{row}$, and oil-gas, $\overline{k}_{rog}$, systems, and (*b*) three-phase (k_{ro}) experiments are depicted in Fig. 3 as functions of oil saturation. Results indicate a clear hysteretic behavior of $\overline{k}_{row}$, when switching from drainage, $\overline{k}_{row}^{D}$, to imbibition, $\overline{k}_{row}^{I}$, conditions.

2.2 Maximum Likelihood model parameter estimation

This section briefly outlines the Maximum Likelihood (ML) framework employed to estimate model parameters and associated bounds of uncertainty in the context of the selected relative permeability models. We introduce the vector $\mathbf{Y}$, whose entries are n true values of $Y_i = \log k_{ro}\left(S_{o,i}\right) = \log k_{ro,i}$, with i = 1, …, n. Vector $\mathbf{Y}^*$ contains n available noisy measurements of Y_i, $Y_i^* = \log k_{ro,i}^*$. For a given model, a ML estimate, $\hat{\boldsymbol{\theta}}$, of vector, $\boldsymbol{\theta}$, whose entries are m model parameters, can be obtained through minimization of the negative log likelihood criterion, *NLL* (e.g., Carrera and Neuman 1986 and references therein)

$$NLL = \frac{J}{\sigma_Y^2} + n\ln(2\pi\sigma_Y^2) \tag{1}$$

where the quantity J is the global residual between model predictions and observations defined as

$$J = \sum_{i=1}^{n} \varepsilon_i^2 ; \qquad \varepsilon_i = Y_i - Y_i^* \tag{2}$$

Here, ε_i is the i-th entry of the prior measurement error vector, which is supposed to be multivariate Gaussian; σ_Y^2 in (1) denotes the measurement error variance. The latter is generally unknown and its ML estimate can be obtained as

$$\hat{\sigma}_Y^2 = \frac{J_{\min}}{n} \tag{3}$$

$J_{\min}$ being the minimum value of J, i.e., $J_{\min} = J\left(\hat{\boldsymbol{\theta}}\right)$. The covariance matrix, $\mathbf{Q}$, of the estimation error is approximated by its Cramer-Rao lower bound as

$$\mathbf{Q} = \hat{\sigma}_Y^2 \left(\mathbf{J}^T \mathbf{J}\right)^{-1} \tag{4}$$

where the superscript T denotes transpose and $\mathbf{J}$ is the $n \times m$ Jacobian matrix whose entries are the derivatives of the target variable, Y_i, with respect to model parameters evaluated at $\hat{\boldsymbol{\theta}}$. We minimize (2) through a gradient method (e.g., Nocedal and Wright 2006), as implemented in the Matlab® environment.

When N_M multiple models are considered for interpretation of the physical scenario of interest, one may minimize (1) for each of the candidate models examined. Once the parameters associated with each model are estimated, the N_M alternative formulations can be ranked by the way of information criteria (e.g., Neuman 2003; Ye et al. 2004, 2008; Khaled et al. 2010; Neuman et al. 2012 and references therein). These include

$$AIC_c = NLL + 2m + \frac{2m(m+1)}{n-m-1} \tag{5}$$

$$BIC = NLL + m \ln n \tag{6}$$

$$KIC = NLL - m \ln(2\pi) - \ln|\mathbf{Q}| \tag{7}$$

Here, AIC_c, BIC and KIC are respectively presented by Hurvich and Tsai (1989), Schwartz (1978) and Kashyap (1982). Models associated with the smallest values of a given criterion are ranked highest. In (7), $\mathbf{Q}$ is typically rendered by (4) (see Ye et al. 2008 for details).

These model discrimination criteria can also be employed to assign posterior probability weights, $p(M_k \mid \mathbf{Y}^*)$, to model M_k conditional on the observation vector $\mathbf{Y}^*$. This posterior probability can be computed according to (Ye et al. 2008)

$$p(M_k \mid \mathbf{Y}^*) = \frac{\exp\left(-\frac{1}{2}\Delta IC_k\right) p(M_k)}{\sum_{i=1}^{N_M} \exp\left(-\frac{1}{2}\Delta IC_i\right) p(M_i)} \tag{8}$$

Here, $\Delta IC_K = IC_K - IC_{\min}$, IC_K being a model discrimination criterion (5)-(7); $IC_{\min}$ is the minimum value of IC_K across the candidate models, and $p(M_k)$ is the prior probability of model M_k. We assign equal prior probability to each model, i.e., $p(M_k) = 1 / N_M$, in the absence of prior information.

We also employ ML Bayesian Model Averaging (BMA) (Neuman 2003; Ye et al. 2004; Tsai 2010) to combine the predictive capabilities of the suite of models considered. Relative permeability values averaged across the model

space and conditional to the available data, $E\left(\mathbf{Y} \mid \mathbf{Y}^*\right)$, can then be calculated by weighting each model through its posterior probability (Ye et al. 2010)

$$E\left(\mathbf{Y} \mid \mathbf{Y}^*\right) = \sum_{k=1}^{N_M} E\left(\mathbf{Y} \mid \mathbf{Y}^*, M_k\right) p\left(M_k \mid \mathbf{Y}^*\right) \tag{9}$$

Mean values (9) are then complemented by the associated variance

$$Var\left(\mathbf{Y} \mid \mathbf{Y}^*\right) = \sum_{k=1}^{N_M} Var\left(\mathbf{Y} \mid \mathbf{Y}^*, M_k\right) p\left(M_k \mid \mathbf{Y}^*\right) + \sum_{k=1}^{N_M} \left[E\left(\mathbf{Y} \mid \mathbf{Y}^*, M_k\right) - E\left(\mathbf{Y} \mid \mathbf{Y}^*\right)\right]^2 p\left(M_k \mid \mathbf{Y}^*\right) \tag{10}$$

$E\left(\mathbf{Y} \mid \mathbf{Y}^*, M_k\right)$ and $Var\left(\mathbf{Y} \mid \mathbf{Y}^*, M_k\right)$ respectively being the posterior mean and variance of $\mathbf{Y}$ computed for model M_k.

2.3 Model parameter identifiability analysis

An important step in a model selection or comparison analysis is the assessment of the identifiability of model parameters, together with their sensitivity to model results and of the way their estimation uncertainty propagates to model outputs. For models exhibiting a nonlinear dependence on their parameters, the boundaries of the confidence region associated with parameter estimates may be characterized by a complex shape and are usually difficult to translate onto uncertainty bounds for model outputs, i.e., relative permeabilities in our study. We assess here identifiability of model parameters through the profile likelihood (PL) technique (Raue et al. 2009). In this context, a given model parameter θ_i is considered to be identifiable if the bounds of uncertainty linked to its estimate, $\hat{\theta}_i$, are associated with a finite width (Raue et al. 2009).

Considering a given set of data, the likelihood of a model conditional to a given value of one of its uncertain parameters, i.e., θ_i, can be assessed by (see also (4) of Raue et al. (2009))

$$\chi^2_{PL}(\theta_i) = \min_{\theta_{j\neq i}}\left[\frac{J(\theta_j)}{\sigma_Y^2}\right] \tag{11}$$

Here, $J(\theta_j)$ is given by (2) where parameter $\theta_{j=i}$ is fixed, we consider a uniform variance of measurement errors, i.e., $\sigma_Y^2 = \hat{\sigma}_Y^2$, and $\chi^2_{PL}(\theta_i)$ is calculated by minimizing J from (2) with respect to all model parameters except $\theta_{j=i}$. As such, one starts by selecting a set of values for θ_i and then minimizes (11) by subsequently conditioning the model to each of these chosen parameter values.

Characterizing parameter uncertainty bounds is also needed to assess (*i*) reliability of model outputs, and (*ii*) sensitivity of each estimated parameter to the model outputs. We consider here bounds of uncertainty identified by introducing a threshold in the likelihood (i.e., the so called PL-based confidence intervals) and defined through a confidence region (Meeker and Escobar 1995)

$$\left\{\theta_i \left| \chi^2_{PL}(\theta_i) - \chi^2_{PL}(\hat{\theta}_i) \leq \Delta_\alpha \right.\right\} \tag{12}$$

Here, $\Delta_\alpha = \chi^2_{PL}(\alpha, df)$ is the α-quantile of the χ^2 distribution with df degrees of freedom. Here, we consider $df = 1$, an approach which renders confidence intervals that hold individually for each of the parameters of a given model. This approach could eventually be employed for model complexity reduction (see, e.g., Raue et al. 2009), an analysis which we do not pursue here, given the relatively simple structure of the models assessed. A confidence interval associated with confidence level α around parameter estimate $\hat{\theta}_i$ indicates that the true value of θ_i^* is comprised within this interval with probability α (Raue et al. 2011). PL-based estimate of the width $\hat{\sigma}^{PL}_{\theta_i}$ of the uncertainty bound corresponds to the range of θ_i values satisfying (12) to the confidence level $\alpha = 0.68$. In Section 3 we compare evaluations of $\hat{\sigma}^{PL}_{\theta_i}$ from (12) to parameter estimate standard deviation, $\hat{\sigma}^{ML}_{\theta_i}$, which constitutes entry of covariance matrix (4) of ML estimation error. Note that intervals of width $\hat{\sigma}^{ML}_{\theta_i}$ around the corresponding ML parameter estimate are symmetric, while confidence intervals calculated on the basis of $\hat{\sigma}^{PL}_{\theta_i}$ are not necessarily so, as we describe in the following.

Depending on the available dataset and the structure of the model under study, one can distinguish between (*i*) identifiability, (*ii*) practical non-identifiability and/or (*iii*) structural non-identifiability of model uncertain parameters. As an illustrative example, Fig. 4 depicts contour plots of $\chi^2_{PL}(\theta_i)$ for a showcase two-dimensional parameter space (θ_1, θ_2) with the aim of illustrating graphically a variety of non-/identifiability conditions for parameter θ_1. Structural non-identifiability, as illustrated in Fig. 4a, results in a perfectly flat region within the range of variability of θ_1 so that (12) would render unbounded confidence intervals in this case. Note that structural non-identifiability arises from model structure, regardless of the quality of the data collected (Cobelli and DiStefano 1980). In the case of practical non-identifiability (see Fig. 4b), $\chi^2_{PL}(\theta_i)$ displays a unique minimum value, but the width of the PL-based confidence interval is of infinite extent along either decreasing or increasing values of θ_i around $\hat{\theta}_i$. Fig. 4c depicts the profile likelihood of an identifiable parameter θ_1. In this example $\chi^2_{PL}(\theta_1)$ displays a unique minimum (at $\hat{\theta}_1$) and is seen to

exceed the threshold value Δ_α for both increasing/ decreasing values of θ_1 around $\hat{\theta}_1$. This indicates that a confidence interval of finite width can be identified for $\hat{\theta}_1$ (see, e.g., Raue et al. 2011 for additional details).

2.4 Three-phase oil relative permeability models analyzed

A variety of empirical/semi-empirical formulations are available and are routinely used for the characterization of three-phase relative permeabilities. Each model may be associated with a set of parameters which can be estimated by model calibration through experiments, i.e., available saturation-relative permeability data. Here, we analyze the behavior of four different models, which we select amongst classical and relatively recent formulations, in terms of their skill to characterize the k_{ro} dataset collected during the SWAG core-flooding experiment presented in Section 2.1. With respect to the work of Ranaee et al. (2016) we do not consider the models of Delshad and Pope (1989) and Lomeland and Ebeltoft (2013) which are associated with a high number of parameters ($m \geq 5$) which is not consistent with the amount of available data for k_{ro} ($n = 6$) in this work (see Fig. 3). The main features of the tested models are briefly described in the following.

2.4.1 Stone model (M_1)

Stone (1970) proposed an empirical model to evaluate three-phase oil relative permeability, k_{ro}, where the maximum value of oil relative permeability in an oil-water system at irreducible water saturation (i.e., in the presence of connate water), $\bar{k}_{row}^{M}$, is set to unity. Here, we consider the modified version (Aziz and Settari 1979)

$$k_{ro} = \frac{\bar{k}_{row}^{I}\bar{k}_{rog}^{D}}{\bar{k}_{row}^{M}} \frac{S_o^N}{\left(1-S_w^N\right)\left(1-S_g^N\right)} \tag{13}$$

where $\bar{k}_{rog}^{D}$ and $\bar{k}_{row}^{I}$ are relative permeabilities of the oil phase observed in two-phase systems, respectively during drainage of gas (in the presence of connate water saturation, $\bar{S}_{wc}$) and imbibition of water; S_w^N, S_o^N and S_g^N are rescaled saturations

$$S_w^N = \frac{S_w - \bar{S}_{wc}}{1-\bar{S}_{wc}-S_{or}}; \quad S_o^N = \frac{S_o - S_{or}}{1-\bar{S}_{wc}-S_{or}}; \quad S_g^N = \frac{S_g}{1-\bar{S}_{wc}-S_{or}} \tag{14}$$

S_w, S_o and S_g respectively being water, oil and gas saturations in a three-phase environment. Note that $\bar{k}_{row}^{I}$ and $\bar{k}_{rog}^{D}$ in (13) are evaluated at oil saturation respectively equal to $(1-S_w)$ and $(1-S_g-\bar{S}_{wc})$. When three-phase data of residual oil saturation, S_{or}, are not available, the value of S_{or} is typically calculated as (Fayers and Matthews 1984)

$$S_{or} = a\bar{S}_{row} + (1-a)\bar{S}_{rog} \qquad \text{with} \qquad a = 1 - \frac{S_g}{1-\bar{S}_{wc}-\bar{S}_{rog}} \tag{15}$$

Here, $\bar{S}_{row}$ and $\bar{S}_{rog}$ represent two-phase residual oil saturations in water-oil and gas-oil systems, respectively. In the presence of three-phase relative permeability data one may consider S_{or} as a model parameter to be estimated through ML. The model parameter vector has only one entry in this case, i.e., $\theta_1 = S_{or}$. Note that the covariance matrix of the estimation error, **Q** (4), for this model reduces to a scalar quantity (i.e., the estimation variance of θ_1, i.e., $\hat{\sigma}_{\theta_1}^2$) that can readily be evaluated analytically as (see also Ranaee et al. 2016)

$$\hat{\sigma}_{\theta_1}^2 = 5.3\left(1-\bar{S}_{wc}-S_{or}\right)^2 \hat{\sigma}_Y^2 \left[\sum_{i=1}^{n}\left[\frac{-1+\bar{S}_{wc}+S_{o,i}}{S_{o,i}-S_{or}} + \frac{S_{w,i}-\bar{S}_{wc}}{1-S_{or}-S_{w,i}} + \frac{S_{g,i}}{1-\bar{S}_{wc}-S_{or}-S_{g,i}}\right]^2\right]^{-1} \tag{16}$$

2.4.2 Baker model (M_2)

Baker (1998) proposed the use of a saturation-weighted interpolation model between (two-phase) oil/water and oil/gas data to evaluate three-phase oil relative permeability. Here, we consider the following modified version of the Baker model, as introduced by Pejic and Maini (2003)

$$k_{ro} = \frac{S_w^N \bar{k}_{row}^{I} + S_g^N \bar{k}_{rog}^{D}}{S_w^N + S_g^N} \tag{17}$$

where

$$S_w^N = \frac{S_w - \bar{S}_{wc}}{1-\bar{S}_{wc}-S_{or}}; \qquad S_g^N = \frac{S_g - \bar{S}_{gt}}{1-\bar{S}_{wc}-\bar{S}_{gt}-S_{or}} \tag{18}$$

This model allows explicit inclusion of the effect of uncertainty of residual oil saturation, S_{or}, on k_{ro}. When three-phase data are not available, S_{or} is usually estimated by (15). Trapped gas saturation is not measured during gas-oil imbibition in the experiments employed in this study. We set it to zero (Spitteri and Juanes 2004) for the purpose of our calculations based solely on two-phase data. In the presence of three-phase data, the two model parameters, $\theta_1 = S_{or}$ and $\theta_2 = \bar{S}_{gt}$, can be estimated via ML as described in Section 2.1. The entries of matrix **Q** are then given by

$$Q_{1,1} = \hat{\sigma}^2_{\theta_1} = \frac{\hat{\sigma}^2_Y}{\left\|\mathbf{J}^T\mathbf{J}\right\|}\sum_{i=1}^{n}\left(\frac{\partial \log k_{ro,i}}{\partial \theta_2}\right)^2 \qquad Q_{2,2} = \hat{\sigma}^2_{\theta_2} = \frac{\hat{\sigma}^2_Y}{\left\|\mathbf{J}^T\mathbf{J}\right\|}\sum_{i=1}^{n}\left(\frac{\partial \log k_{ro,i}}{\partial \theta_1}\right)^2 \tag{19}$$

$$Q_{1,2} = Q_{2,1} = -\frac{\hat{\sigma}^2_Y}{\left\|\mathbf{J}^T\mathbf{J}\right\|}\sum_{i=1}^{n}\frac{\partial \log k_{ro,i}}{\partial \theta_1}\frac{\partial \log k_{ro,i}}{\partial \theta_2} \tag{20}$$

where

$$\left\|\mathbf{J}^T\mathbf{J}\right\| = \sum_{i=1}^{n}\left(\frac{\partial \log k_{ro,i}}{\partial \theta_1}\right)^2\sum_{i=1}^{n}\left(\frac{\partial \log k_{ro,i}}{\partial \theta_2}\right)^2 - \left[\sum_{i=1}^{n}\frac{\partial \log k_{ro,i}}{\partial \theta_1}\frac{\partial \log k_{ro,i}}{\partial \theta_2}\right]^2 \tag{21}$$

2.4.3 Model M_3 (Du et al. 2004)

Du et al. (2004) introduced the following model

$$k_{ro} = \frac{\left(S_w - \overline{S}_{wc}\right)\left(S_w + AS_g\right)}{\left(S_w + S_g - \overline{S}_{wc}\right)}\overline{k}^I_{row} + \frac{S_g\left(B\left(S_w - \overline{S}_{wc}\right) + S_g\right)}{\left(S_w + S_g - \overline{S}_{wc}\right)}\overline{k}^D_{rog} \tag{22}$$

In the presence of three-phase data, the two model parameters $\theta_1 = A$ and $\theta_2 = B$ can be estimated via ML. The entries of matrix **Q** are given by (19) and (20) and $\left\|\mathbf{J}^T\mathbf{J}\right\|$ are calculated according to (21). According to Du et al. (2004), the parameters A and B are typically set to 0.9 and 0.95, respectively, in the absence of three-phase data.

2.4.4 Sigmoid model (M_4)

Ranaee et al. (2015) proposed to evaluate k_{ro} by a Sigmoid model. Considering the high content of the water phase in the SWAG injection system, we employ the following formulation

$$k_{ro} = \frac{\left(S_w - \overline{S}_{wc}\right)k^S_{ro} + \left(S_g - \overline{S}_{gt}\right)\overline{k}^D_{rog}}{\left(S_w - \overline{S}_{wc}\right) + \left(S_g - \overline{S}_{gt}\right)} \tag{23}$$

where k^S_{ro} is given by

$$k^S_{ro} = \frac{\overline{k}^M_{row}S_o}{\overline{S}^M_{ow} + \exp\left[\lambda - \beta\left(\frac{S_o}{\overline{S}^M_{ow}}\right)^{\overline{S}^M_{ow}}\right]} \tag{24}$$

Here, $\bar{S}_{ow}^{M}$ is the largest oil saturation observed in a two-phase (oil-water) system in the presence of connate water; λ and β are the two model parameters. It should be noted that parameters λ and β can be directly calculated solely on the basis of two-phase (oil-gas and oil-water) data (Ranaee et al. 2015) as

$$\lambda = \ln\left[\frac{\bar{k}_{row}^{M} S_o^{inf}}{k_{ro}^{inf}} - \bar{S}_{ow}^{M}\right] + \beta\left(\frac{S_o^{inf}}{\bar{S}_{ow}^{M}}\right)^{\bar{S}_{ow}^{M}}; \qquad \beta = \frac{1}{\bar{S}_{ow}^{M}}\left(\frac{m_{inf} S_o^{inf}}{k_{ro}^{inf}} - 1\right)\left(1 - \frac{\bar{S}_{ow}^{M} k_{ro}^{inf}}{\bar{k}_{row}^{M} S_o^{inf}}\right)^{-1}\left(\frac{S_o^{inf}}{\bar{S}_{ow}^{M}}\right)^{-\bar{S}_{ow}^{M}} \tag{25}$$

with

$$S_o^{inf} = \bar{S}_{row} + \frac{\bar{S}_{ow}^{M} - \bar{S}_{row}}{2}; \qquad k_{ro}^{inf} = \bar{k}_{row}^{I}\left(S_o^{inf}\right); \qquad m_{inf} = \left.\frac{\partial \bar{k}_{row}^{I}}{\partial S_o}\right|_{S_o^{inf}} \tag{26}$$

i.e., m_{inf} is the slope of $\bar{k}_{row}^{I}$ at S_o^{inf}.

Similar to the other models analyzed, in the presence of three-phase data parameters $\theta_1 = \lambda$ and $\theta_2 = \beta$ can be estimated through ML, the entries of matrix **Q** are given by (19) and (20), and $\left\|\mathbf{J}^T\mathbf{J}\right\|$ is calculated from (21).

3 Results and discussion

We illustrate here the results of the analysis based on ML calibration to the available dataset of the four interpretive models described in Section 2.4. We also frame our analysis in the context of the ML Bayesian Model Averaging (BMA) approach. Identifiability of model parameters is evaluated through the Profile Likelihood (PL) technique detailed in Section 2.3.

Fig. 5 depicts results obtained (*i*) by calculating k_{ro} relying solely on information from two-phase data (Fig. 5a) and (*ii*) by ML calibration of models M_1 - M_4 relying on three-phase data (Fig. 5b). Table 1 lists values of (*i*) Mean Square Difference *MSD=J / n*, where *J* is calculated from (2) and represents the discrepancy between model calculations on two-phase information and three-phase k_{ro} data; and (*ii*) $\hat{\sigma}_Y^2$ estimates of measurement errors (3) obtained from ML calibration of the models on the available three-phase relative permeability data. The Table also lists ML model parameter estimates, ML- and PL-based confidence intervals together with the resulting characterization of model parameter identifiability.

Visual inspection of Fig. 5a and Fig. 5b suggests that models M_2 and M_4 yield quite reasonable estimates of k_{ro} through the entire range of saturations even when relying solely on two-phase information. Model M_1 tends to overestimate k_{ro} for high oil saturations, while rendering values of *MSD* and $\hat{\sigma}_Y^2$ which are similar to those of M_2 and M_4. The quality of the results tends to improve when parameters of models M_1, M_3 and M_4 are estimated through ML on three-phase data. Otherwise, ML calibration does not lead to improving the results associated with model M_2.

We then analyze the entries of the covariance matrix **Q** (4) associated with each of the tested models. Fig. 6a depicts normalized uncertainty intervals, quantified by $(\hat{\theta}_j + \hat{\sigma}_{\theta_j})/\hat{\theta}_j$, for all ML model parameter estimates. We can observe that ML estimates of the parameters of model M_4 are associated with the smallest (normalized) uncertainty, estimates of model M_2 parameters (S_{or} and $\bar{S}_{gt}$) being linked to the largest estimation uncertainties.

We also rely on local sensitivity analysis to address relative sensitivity of parameter estimates to model responses (for each k_{ro} data point). Fig. 6b illustrates normalized model sensitivities calculated at the ML optimum for each of the available relative permeability ($k^*_{ro,i}$) data. These results show that ML-based model parameter sensitivities are virtually zero for the highest values of $k^*_{ro,i}$. This result might be related to the selected structure of the objective function (2), which is formulated in terms of the logarithms of model responses and available observations. It is clear that the parameters associated with the sigmoid model M_4 are associated with the highest sensitivity, for the small to intermediate oil saturation values. These results support the earlier observation of Ranaee et al. (2016) about the ability of this model to represent the observed system behavior.

We now employ the PL technique described in Section 2.3 to investigate identifiability of model uncertain parameters. Fig. 7 depicts the profile likelihood of all model parameters (i.e., S_{or} for M_1; S_{or}, and $\bar{S}_{gt}$ for M_2; A, and B for M_3; and λ, and β for M_4) estimated by (11). The upper and lower horizontal dashed lines represent Δ_α thresholds of the χ^2- distribution with values of α = 0.68 and 0.95, respectively representing width of PL-based confidence intervals equal to $\hat{\sigma}^{PL}_{\theta_i}$ or $2\hat{\sigma}^{PL}_{\theta_i}$, as calculated from (12).

The results of Fig. 7a are indicative of practical non-identifiability of the model parameter, the profile likelihood displaying the same features of Fig. 4b (in this case for both values of α considered). This finding indicates that the amount and/or quality of the available experimental dataset do not contain enough information to yield an estimate of S_{or} of model M_1 with bounded confidence interval at α = 0.68.

Parameter S_{or} of model M_2 exhibits structural non-identifiability (see Fig. 7b). Estimation of $\chi^2_{PL}\left(S_{or}\right)$ results in a perfectly flat valley and the profile likelihood does not reach to the Δ_α threshold, so that PL-based confidence interval is unbounded. The PL-based confidence interval of parameter $\bar{S}_{gt}$ of model M_2 is unbounded along the direction of decreasing values of $\bar{S}_{gt}$, the profile likelihood exceeding the Δ_α threshold solely in the increasing direction of $\bar{S}_{gt}$ values (see Fig. 7c). This finding indicates practical non-identifiability of this parameter on the basis of the available dataset. Note that $\bar{S}_{gt}$ is not necessarily an uncertain parameter in the structure of model M_2 (see Ranaee et al. 2016). We treat it as such in our study because it was not measured in the context of the experimental campaign we rely upon.

Profile likelihood analyses of models M_3 and M_4 reveal identifiability (structural and practical) of the model parameters because (*i*) the normalized profile likelihood of all parameters exceed the threshold of Δ_α yielding confidence interval of finite size and (*ii*) a clear minimum is attained (Figs. 7 d-g).

As discussed above, Table 1 lists PL-based confidence intervals for $\alpha = 0.68$ ($\hat{\theta}_i \pm \hat{\sigma}^{PL}_{\theta_i}$) together with their ML-based counterparts, $\hat{\theta}_i \pm \hat{\sigma}^{ML}_{\theta_i}$. ML- and PL-based estimates of confidence intervals are similar for identifiable parameters (see Table 1). Otherwise, the PL-based results are consistent with the large bounds of uncertainty associated with ML in the presence of parameter non-identifiability. Note that PL-based confidence intervals are not necessarily symmetric with respect to the estimated parameter. The latter feature is typically considered as a shortcoming of ML results, which are based on (4), especially in cases where complex shapes of parameter confidence regions can arise from nonlinear model dependence on its parameters (see also, e.g., Joshi et al. 2006 and references therein).

Fig. 8a depicts model selection criteria evaluated from the ML model calibration results. We observe that most model criteria favor the use of model M_4 for the interpretation of the available three-phase k_{ro} data. These results are in agreement with our previous work (see Ranaee et al. 2016), based on diverse injection scenarios and different characteristics of the fluids and core sample.

Fig. 8b depicts the posterior model weight (for AIC_c) and probability (for *BIC* and *KIC*), $p\left(M_k \mid \mathbf{Y}^*\right)$, for each candidate model. In our analysis we assign an equal prior probability to each candidate model, i.e., $p\left(M_k\right) = 1 / N_M$ (k = 1,..., 4). The highest posterior probability/ weight is always assigned to model M_4, with the only exception of the results associated with the use of AIC_c from (5). Note that AIC_c and *BIC* tend to favor models solely on the basis of their number of parameters. Therefore, these criteria give high posterior weights to model M_1. Otherwise, *KIC* from (7) tends

to favor models with relatively small expected information content per observation (e.g., Hernandez et al. 2006; Ye et al. 2008; Riva et al. 2011), in the presence of alternative models associated with the same number of parameters, equal minima for *NLL*, and the same prior probability. As such, *KIC* assigns a non-negligible probability to model M_2, consistent with the associated values of the entries of **Q**, resulting in a relatively high uncertainty of parameter estimates (see Fig. 6a).

Our analysis is complemented by Fig. 8c, which depicts results obtained solely on the basis of models M_3 and M_4, the parameters of models M_1 and M_2 being associated with structural/practical non-identifiability. In this case, our results unequivocally reveal that model M_4 is always associated with a posterior model weight/probability which exceeds 90%.

Maximum Likelihood BMA is finally employed to provide a multi-model analysis of the oil relative permeability data. We use (9)-(10) to compute ML BMA estimates and associated variances. Fig. 9 depicts scatterplots of BMA estimates versus observations of $Y^* = \log k_{ro}^*$ when replacing *IC* in (8)-(10) with (a) *NLL*, (b) AIC_c, (c) *BIC* and (d) *KIC*. We include results of BMA estimates obtained by considering all candidate models tested (denoted as $E\left(\mathbf{Y} \mid \mathbf{Y}^*\right)$ in the figure) as well as those based solely on models M_3 and M_4, whose parameters are not affected by non-identifiability issues (denoted as $E\left(\tilde{\mathbf{Y}} \mid \mathbf{Y}^*\right)$ in the figure). Fig. 9 also depicts intervals of width $E\left(\mathbf{Y} \mid \mathbf{Y}^*\right) \pm \sqrt{Var\left(\mathbf{Y} \mid \mathbf{Y}^*\right)}$ as an additional term of comparison to characterize the uncertainties associated with BMA estimates. Corresponding $E\left(\tilde{\mathbf{Y}} \mid \mathbf{Y}^*\right) \pm \sqrt{Var\left(\tilde{\mathbf{Y}} \mid \mathbf{Y}^*\right)}$ bounds of uncertainties are included when considering BMA limited to models M_3 and M_4.

Generally, estimates of $\log k_{ro}^*$ from $E\left(\tilde{\mathbf{Y}} \mid \mathbf{Y}^*\right)$ are very similar to those obtained from $E\left(\mathbf{Y} \mid \mathbf{Y}^*\right)$. This indicates a very limited effect of the models with embedded non-identifiable parameters to improve predictions, a finding which is also in line with the small posterior probability associated with these latter models. It is then noted that uncertainties associated with the averaged model based solely on identifiable candidates are slightly higher than those related to averaged model considering all candidates, i.e., $Var\left(\mathbf{Y} \mid \mathbf{Y}^*\right) \leq Var\left(\tilde{\mathbf{Y}} \mid \mathbf{Y}^*\right)$. These results clearly satisfy possibility of reducing candidate models of k_{ro} estimation to the identifiable ones which can extensively reduce computational costs of implementing averaged model.

4 Concluding remarks

Our work leads to the following key conclusions.

1. Models provide reasonable results in reproducing three-phase oil relative permeability data when calculations are based on information from two-phase data. According to Ranaee et al (2016) this similar behavior of the tested models is due to initiation of the three-phase experiment under SWAG injection at high oil saturation.
2. Implementation of ML calibration leads to some improvements in estimations of k_{ro}. In this case, AIC_c prefers M_1 (Stone 1970) model, while the other discrimination criteria prefer M_4 (Ranaee et al. 2015) model. The disagreement between different information criteria is expected to be due to small size of available dataset. Then AIC_c tends to select less complex models (see e.g., Ye et al. 2008) and *KIC* favors models with relatively small expected information content per observation (e.g., Hernandez et al. 2006, Ye et al. 2008, and Riva et al. 2011).
3. In general, $\hat{\sigma}_Y^2$ values are reported smaller than those of *LMSE* since three-phase data are considered in the model calibrations. This evidences general efficiency of ML calibration of the models on three-phase data. However, comparing the performance of each individual model in reproducing data, we can state that M_4 is more favorable to estimate k_{ro} even if characterization of the model bases solely on information from two-phase data.
4. Estimation of k_{ro} from M_3 and M_4 models show reasonable sensitivity to the variation of the related uncertain parameters particularly at low oil saturation values. On the other hand, ML estimation of the calibration parameters of M_2 model involves extensively high uncertainties. These issues point the need of identifiability analysis on parameters of candidate modes to the available dataset.
5. Profile Likelihood (PL) technique seems to be a powerful approach to evaluate non-/identifiable parameters. The latter allows detecting both structural and practical identifiability of uncertain parameter(s), so that leading reliable model predictions.

Acknowledgments

Authors are grateful for the partial financial support from Eni SpA.

References

Alizadeh A H and Piri M (2014a) Three-phase flow in porous media: A review of experimental studies on relative permeability. Rev Geophys 52:468-521. doi:10.1002/2013RG000433

Alizadeh A H and Piri M (2014b) The effect of saturation history on three-phase relative permeability: An experimental study. Water Resour Res 50:1636-166. doi:10.1002/2013WR014914

Aziz K and Settari A (1979) Petroleum reservoir simulation. Applied Science Publishers, London.

Baker L E (1988) Three phase relative permeability correlation. SPE 17369 proceedings of the SPE/DOE Symposium on Enhanced Oil Recovery, April 17-20, Tulsa, USA.

Blunt M J (2000) An empirical model for three-phase relative permeability. SPE J 5:435-445. doi:10.2118/67950-PA

Carrera J, Neuman S P (1986). Estimation of aquifer parameters under transient and steady state conditions: 1. Maximum likelihood method in cooperating prior information. Water Resour Res 22(2):199-210. doi:10.1029/WR022i002p00199

Cobelli C and DiStefano III J (1980) Parameter and structural identifiability concepts and ambiguities: a critical review and analysis. Am J Physiol Regul Integr Comp Physiol 239:7-24.

Delshad M and Pope G A (1989) Comparison of the three-phase oil relative permeability models. Transp Porous Med 4:59-83. doi:10.1007/BF00134742

Du Y, Bolaji O B, and Li D (2004) Literature review on methods to obtain relative permeability data. 5th Conference and Exposition on Petroleum Geophysics Hyderabad India 15-17 January.

Fayers F Jand J D Matthews (1984) Evaluation of normalized Stone's methods for estimating three-phase relative permeabilities. SPE J 24(02):224-232. doi:10.2118/11277-PA

Flassig R J, Migal I, Der Zalm Ev, Rihko-Struckmann L, Sundmacher K (2015) Rational selection of experimental readout and intervention sites for reducing uncertainties in computational model predictions. BMC Bioinformatics 16:16-13. doi:10.1186/s12859-014-0436-5

Hernandez A F, Neuman S P, Guadagnini A, Carrera J (2006) Inverse stochastic moment analysis of steady state flow in randomly heterogeneous media. Water Resour Res 42(5):W05425. doi:10.1029/2005WR004449

Hurvich C M and Tsai C L (1989) Regression and time series model selection in small samples. Biometrika 76:297-307.

Kashyap R L (1982) Optimal choice of ar and ma parts in autoregressive moving average models. IEEE Transactions on Pattern Analysis and Machine Intelligence PAMI 4(2): 99-104.

Khaled H, Ataur R (2010) Selection of the best fit flood frequency distribution and parameter estimation procedure: a case study for Tasmania in Australia. Stochastic Environ Res Risk Assess, 25(3):415-428. doi:10.1007/s00477-010-0412-1

Joshi M, Seidel-Morgenstern A and Kremling A (2006) Exploiting the bootstrap method for quantifying parameter confidence intervals in dynamical systems. Metab Eng 8:447-455. doi:10.1016/j.ymben.2006.04.003

Kreutz C, Raue A, and Timmer J (2012) Likelihood based observability analysis and confidence intervals for predictions of dynamic models. BMC Systems Biology 6(1):120

Lomeland F, and Ebeltoft E (2013) Versatile three-phase correlations for relative permeability and capillary pressure. International Symposium of the Society of Core Analysts, Napa Valley, California, USA, 16-19 September.

Meeker W and Escobar L (1995) Teaching about approximate confidence regions based on maximum likelihood estimation. Am Stat 49(1):48-53. doi:10.2307/2684811

Moghadasi L, Guadagnini A, Inzoli F, Bartosek M, and Renna D (2016) Characterization of Two- and Three-Phase Relative Permeability of Water-Wet Porous Media through X-Ray Saturation Measurements. J Petrol Sci Eng 138:1-15. doi:10.1016/j.petrol.2016.05.031

Moghadasi L, Guadagnini A, Inzoli F and Bartosek M (2015) Interpretation of Two-Phase Relative Permeability Curves through Multiple Formulations and Model Quality criteria. J Petrol Sci Eng 135:738-749. doi:10.1016/j.petrol.2015.10.027

Neuman S.P (2003). Maximum likelihood Bayesian averaging of uncertain model predictions. Stochastic Environ Res Risk Assess, 17(5):291-305. doi:10.1007/s00477-003-0151-7

Neuman S P, Xue L, Ye M, and Lu D (2012) Bayesian analysis of data-worth considering model and parameter uncertainties. Adv Water Resour 36:75-85. doi:10.1016/j.advwatres.2011.02.007.

Nocedal and Wright S J (2006) Numerical optimization. 2nd Ed Springer Verlag.

Oak M J (1990) Three-phase relative permeability of water-wet Berea. SPE-20183, 7th SPE/DOE Enhanced Oil Recovery Symposium, Tulsa, Oklahoma, 22-25 April. doi:10.2118/20183-MS

447 Pejic D and Maini B B (2003) Three-phase relative permeability of petroleum reservoirs. SPE 81021, SPE Latin
448 American and Caribbean Petroleum Engineering Conference, Trinidad, 27-30 April. doi:10.2118/81021-MS

449 Ranaee E, Riva M, Porta G M, and A Guadagnini (2016) Comparative assessment of three-phase oil relative
450 permeability models. Water Resour Res 52(7):5341-5356. doi:10.1002/2016WR018872

451 Ranaee E, Porta G M, Riva M, Blunt M J and Guadagnini A (2015) Prediction of three-phase oil relative permeability
452 through a sigmoid-based model. J Petrol Sci Eng 126:190-200. doi:10.1016/j.petrol.2014.11.034

453 Raue A, Kreutz C, Maiwald T, Bachmann J, Schilling M, Klingmuller U and Timmer J (2009) Structural and practical
454 identifiability analysis of partially observed dynamical models by exploiting the profile likelihood. Bioinformatics
455 25(15):1923-1929. doi:10.1093/bioinformatics/btp358

456 Raue A, Kreutz C, Maiwald T, Klingmüller U, Timmer J (2011) Addressing parameter identifiability by model-based
457 experimentation. IET Syst Biol 5(2):120-30. doi:10.1049/iet-syb.2010.0061

458 Riva M, Panzeri M. Guadagnini A, and Neuman S P (2011) Role of model selection criteria in geostatistical inverse
459 estimation of statistical data- and model-parameters. Water Resour Res 47(7):W07502.
460 doi:10.1029/2011WR010480

461 Schwarz G E. (1978) Estimating the dimension of a model. Annals of Statistics 6(2):461-464.

462 Silpngarmlers N, Guler B, Ertekin T and Grader A S (2002) Development and testing of two-phase relative
463 permeability predictors using artificial neural networks. SPE J 7(03):299-308. doi:10.2118/79547-PA

464 Spiteri E J and Juanes R (2004) Impact of relative permeability hysteresis on the numerical simulation of WAG
465 injection. J Petrol Sci Eng 50:115-139. doi:10.1016/j.petrol.2005.09.004

466 Stone H L (1970) Probability model for estimation of three-phase relative permeability. J Petrol Tech 22:214-218.

467 Tsai F T C (2010) Bayesian model averaging assessment on groundwater management under model structure
468 uncertainty. Stochastic Environ Res Risk Assess 24(6):1436-3259. doi:10.1007/s00477-010-0382-3

469 Tiedeman C R, Ely D M, Hill M C, and O'Brien G M (2004) A method for evaluating the importance of system state
470 observations to model predictions, with application to the Death Valley regional groundwater flow system. Water
471 Resour Res 40(12)W12411. doi:10.1029/2004WR003313

Tiedeman C R, Hill M C, D'Agnese F A, and Faunt C C (2003) Methods for using groundwater model predictions to guide hydrogeologic data collection, with application to the Death Valley regional ground-water flow system. Water Resour Res 39(1):1-17. doi:10.1029/2001WR001255

Ting H. Yonghua Z, Haishen L, Edward S, Zhongbo Y, Fen O (2015) Parameter sensitivity analysis and optimization of Noah land surface model with field measurements from Huaihe River Basin, China. Stochastic Environ Res Risk Assess 29(5):13831401. doi:10.1007/s00477-015-1033-5

Ye M, Neuman S P, and Meyer P D (2004) Maximum likelihood Bayesian averaging of spatial variability models in unsaturated fractured tuff. Water Resour Res 40(5):W05113. doi:10.1029/2003WR002557

Ye M, Meyer P D, and Neuman S P (2008) On model selection criteria in multimodel analysis. Water Resour Res 44(3): W03428. doi:10.1029/2008WR006803

Ye M, Pohlmann K F, Chapman J B, Pohll G M, Reeves D M (2010) A model averaging method for assessing ground water conceptual model uncertainty. Ground water 48(5):716-728. doi:10.1111/j.1745-6584.2009.00633.x

485

486 **Table 1** Results in terms of $MSD = J/n$ when calculations rely upon information from two-phase data; measurement

487 error variance ($\hat{\sigma}_Y^2$) when modeling includes information from three-phase data. ML-based ($\hat{\theta}_i \pm \hat{\sigma}_{\theta_i}^{ML}$) and PL-based (

488 $\hat{\theta}_i \pm \hat{\sigma}_{\theta_i}^{PL}$) confidence intervals associated with estimation of θ_i from each candidate model.

Models	*MSD*	$\hat{\sigma}_Y^2$	θ_i	$\hat{\theta}_i$	*ML-based confidence interval*		*PL-based confidence interval*		*Non-identifiability*
					$\hat{\theta}_i - \hat{\sigma}_{\theta_i}^{ML}$	$\hat{\theta}_i + \hat{\sigma}_{\theta_i}^{ML}$	$\hat{\theta}_i - \hat{\sigma}_{\theta_i}^{PL}$	$\hat{\theta}_i + \hat{\sigma}_{\theta_i}^{PL}$	
M_1 (Stone, 1970)	0.047	0.037	S_{or}	0.045	-0.046	+0.135	-∞	+0.103	Practical
M_2 (Baker, 1988)	0.075	0.075	S_{or}	0.11	-5349	+5349	-∞	+∞	Structural
			$\overline{S}_{gt}$	1.72×10^{-4}	-0.021	+0.021	-∞	+0.17	Practical
M_3 (Du et al, 2004)	0.202	0.095	A	1.66	-2.985	+6.297	-1.62	+7.2	Identifiable
			B	8.78	-4.505	+22.07	+1.23	+27	Identifiable
M_4 (Ranaee et al, 2015)	0.059	0.023	λ	5.44	+1.532	+9.350	+0.99	+14.5	Identifiable
			β	16.46	+1.851	+31.07	+1.99	+54	Identifiable

489

490

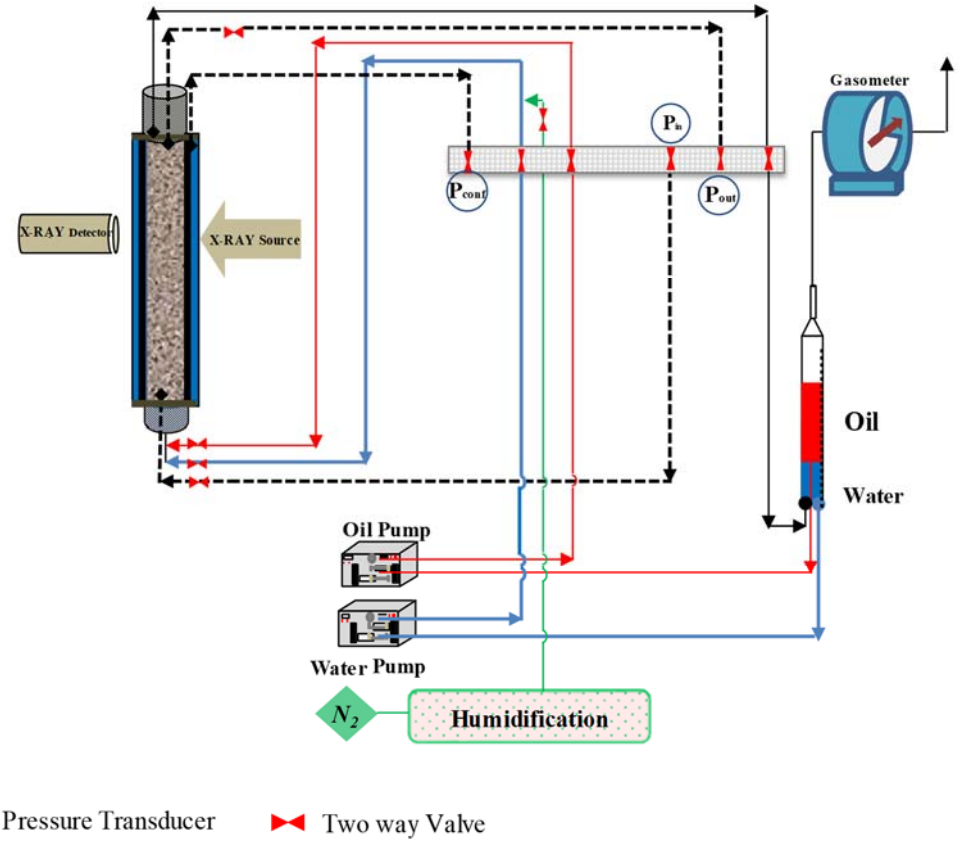

Fig. 1 Sketch of experimental setup; adapted from Moghadasi et al. (2016).

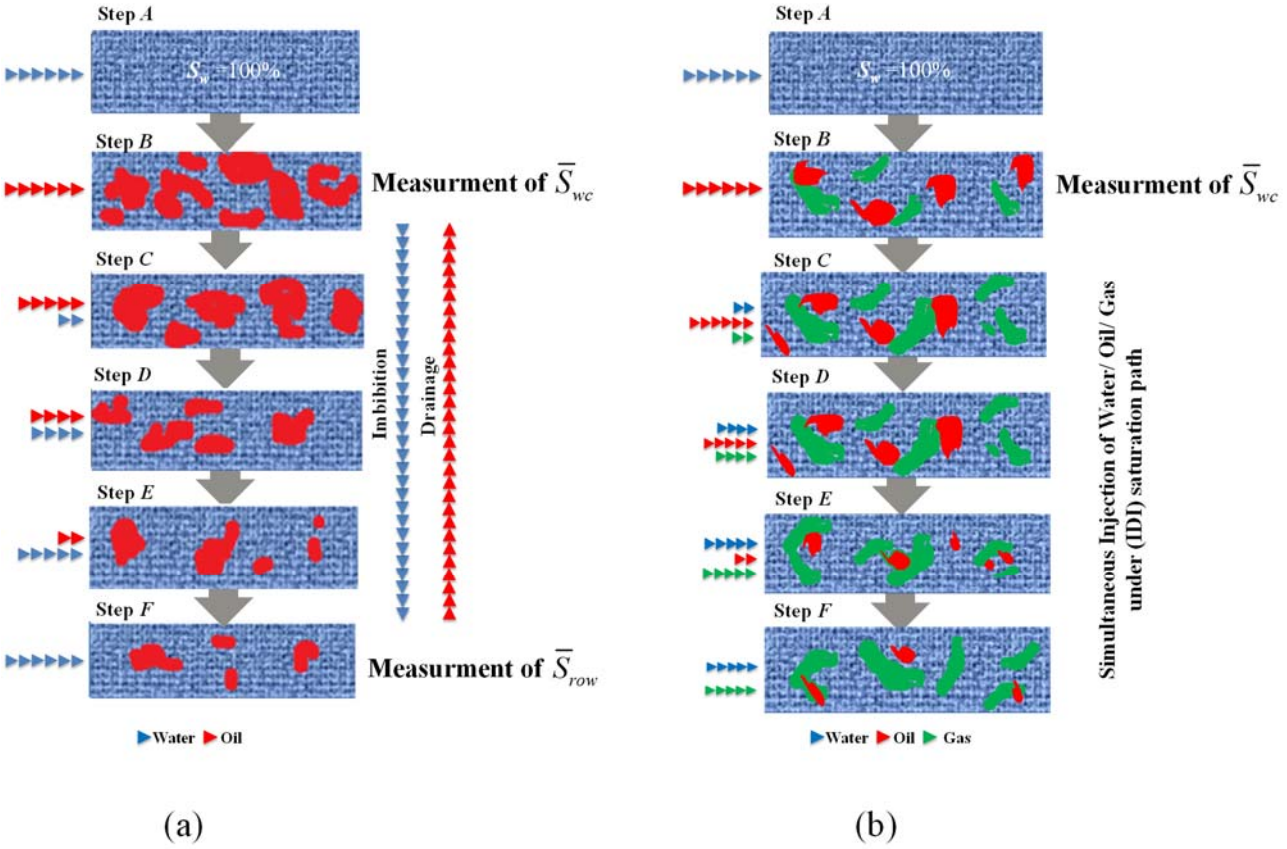

Fig. 2 Main steps of the procedure employed for Steady-State (SS) (a) two- and (b) three-phase core-flooding experiments (Moghadasi et al. 2016).

500

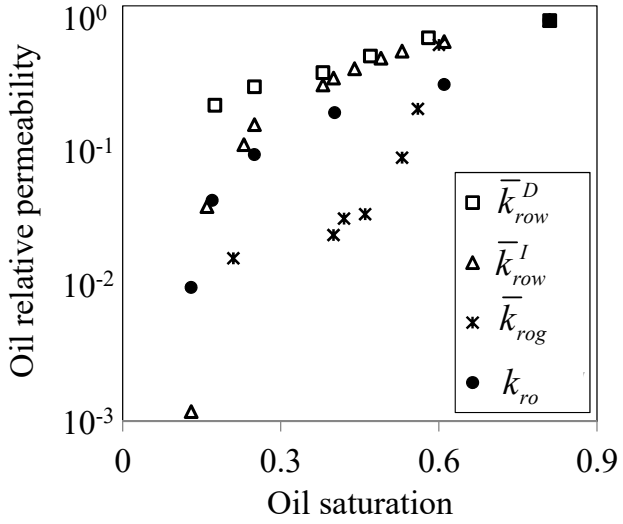

501

502 **Fig. 3** Two- and three-phase oil relative permeability data versus oil saturation.

503

504

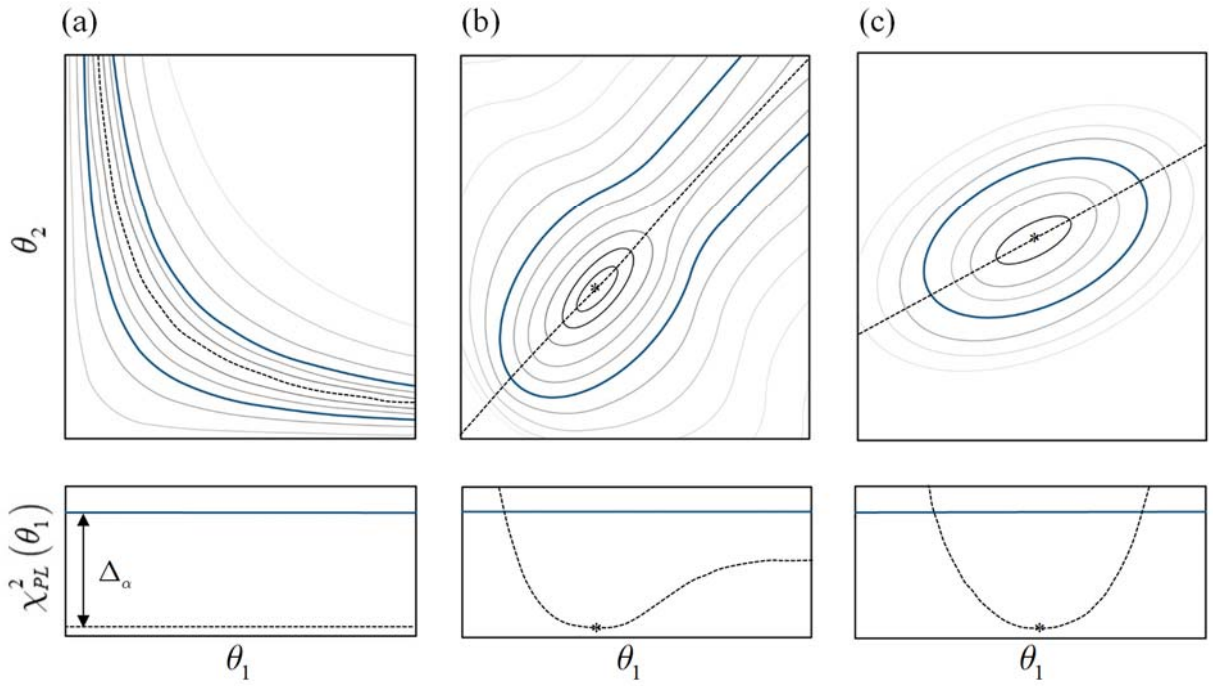

505

506 **Fig. 4** Schematic contour plots of objective function (2) for two-dimensional parameter space of a generic model
507 representing (a) structural non-identifiability; (b) practical non-identifiability; and (c) both parameters are identifiable.
508 The star represents the ML estimate in the parameter space, bold line displays the threshold Δ_α from (12) utilized to
509 assess PL-based confidence interval/region for a confidence level α and the dashed line indicates the profile likelihood
510 (11) of the parameter θ_1 (see Raue et al. 2011 for more details).

511

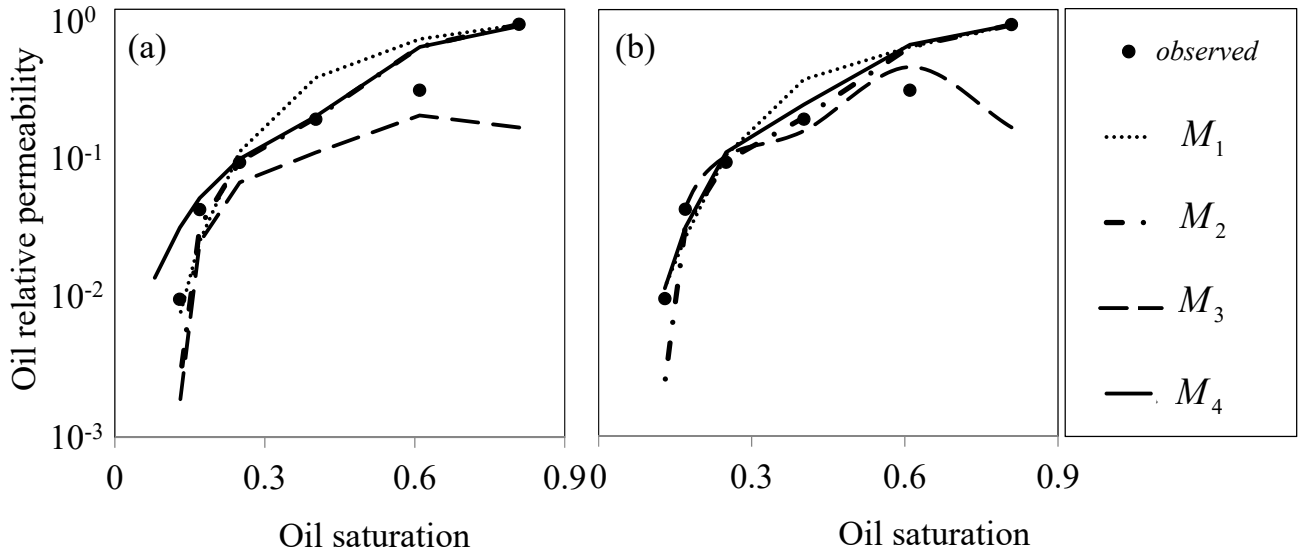

Fig. 5 Three-phase oil relative permeability versus oil saturation. Curves represent values calculated through M_1, M_2, M_3, and M_4 models (a) solely on information from two-phase data and (b) ML calibrated on three-phase data.

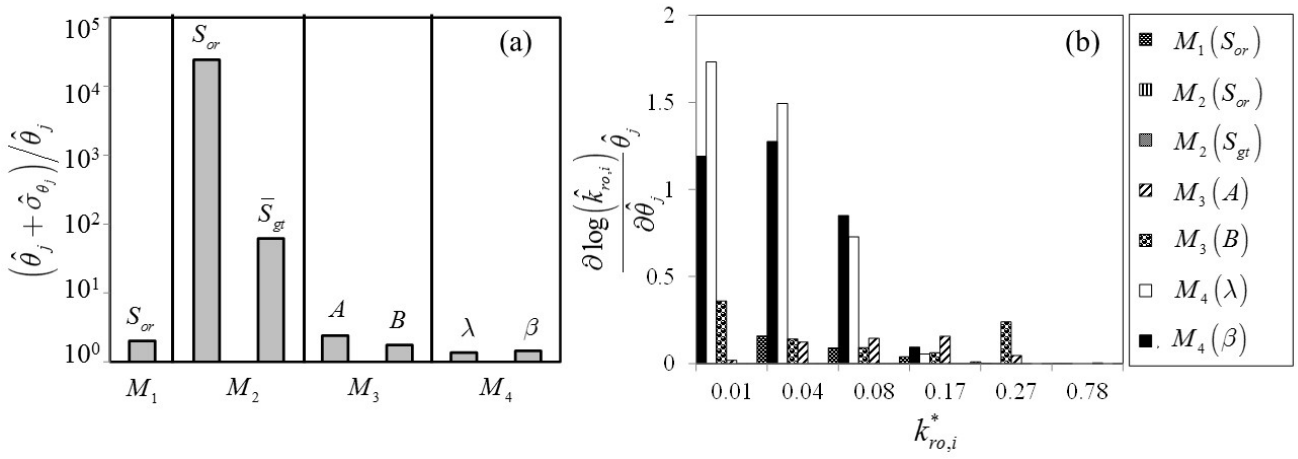

Fig. 6 (a) Normalized uncertainty bounds quantified by $(\hat{\theta}_j+\hat{\sigma}_{\theta_j})/\hat{\theta}_j$ for all parameter estimates $\hat{\theta}_j$ resulting from ML calibration of the models (b) local sensitivity of $\hat{Y}_i=\log\hat{k}_{ro,i}$ at *i*th measurements resulted from ML calibrated models normalized with the value of $\hat{\theta}_j$.

523

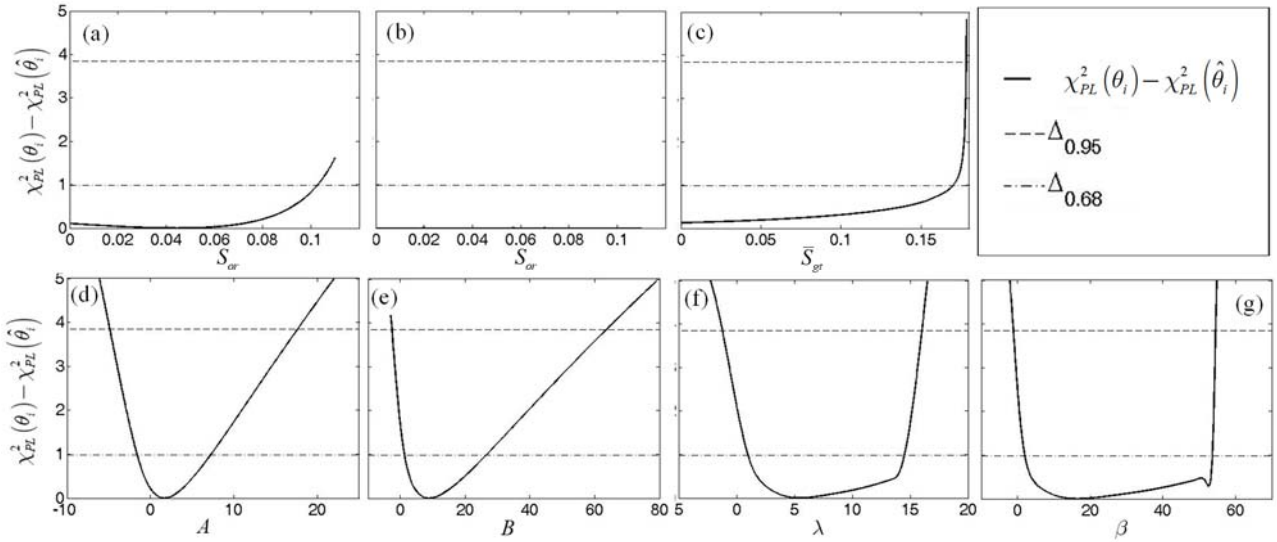

524

525 **Fig. 7** The bold line indicates the normalized profile likelihood from (11) versus calibration parameters of (a) S_{or} of M_1

526 model; (b) S_{or} and (c) $\bar{S}_{gr}$ of M_2 model; (d) A and (e) B of M_3 model and (f) λ and (g) β of M_4 model. The dashed

527 lines display the threshold Δ_α from (12) for confidence levels of α = 0.68 and 0.95.

528

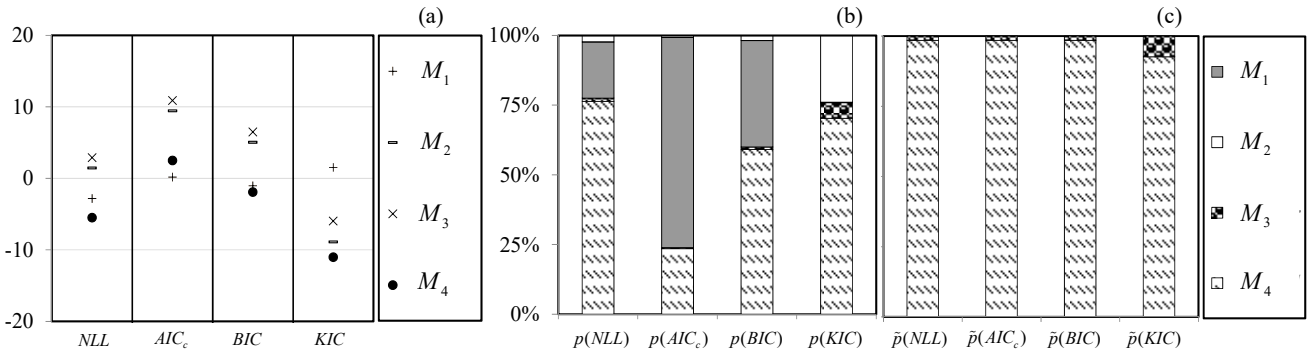

Fig. 8 (a) Model selection criteria evaluated based on ML calibration of studied three-phase oil relative permeability models on available measurements. Posterior model weight (for *NLL* and AIC_c) and model probability (for *BIC* and *KIC*) evaluated for (b) all considered models (c) solely identifiable models.

535

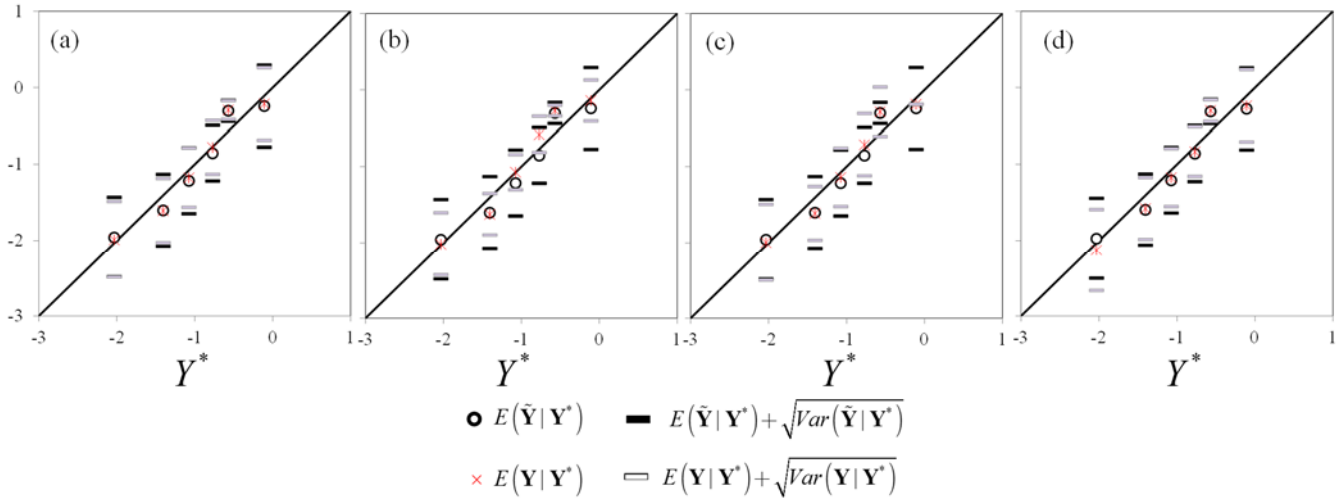

536

537 **Fig. 9** Estimates of k_{ro} versus experimental values and *IC*= (a) *NLL*; (*b*) AIC_c; (*c*) *BIC*; and (*d*) *KIC*.

538

539